Activation of Methane by Neutral Transition Metal Oxides (ScO, NiO, and PdO): A Theoretical Study

Der-Yan Hwang*,† and Alexander M. Mebel*,‡

Department of Chemistry, Tamkang University, Tamsui 25137, Taiwan, and Institute of Atomic and Molecular Sciences, Academia Sinica, P. O. Box 23-166, Taipei 10764, Taiwan

Received: June 30, 2002; In Final Form: September 26, 2002

Density functional B3LYP calculations have been employed to investigate potential energy surfaces for the reactions of scandium, nickel, and palladium oxides with methane. The results show that NiO and PdO are reactive toward methane and can form molecular complexes with CH_4 bound by 9−10 kcal/mol without a barrier. At elevated temperatures, the dominant reaction channel is direct abstraction of a hydrogen atom by the oxides from CH_4 with a barrier of ∼16 kcal/mol leading to MOH (M = Ni, Pd) and free methyl radical. A minor reaction channel is an insertion into a C−H bond to produce CH_3MOH molecules via transition states lying 19−20 kcal/mol above the initial reactants. For instance, for PdO, the rate constant of the hydrogen abstraction channel evaluated using the transition state theory for the 300−1000 K temperature range, $k_{methyl} = 7.12 \times 10^{-11} \exp(-17\,329/RT)$ cm^3 s^{-1} molecule^{-1}, is 2−3 orders of magnitude higher than the insertion rate constant and the branching ratio for the PdOH + CH_3 products is 98−99%. The preferable channel of dissociation of CH_3NiOH is a cleavage of the Ni−C bond leading to the radical NiOH + CH_3 products without an exit barrier, while CH_3PdOH is more likely to undergo 1,2-CH_3 migration to produce a $PdCH_3OH$ complex and eventually Pd plus methanol. PdOH and CH_3 can recombine producing CH_3PdOH and isomerization, and dissociation of this molecule results in further transformation of methyl radical into methanol. However, the NiOH + CH_3 reaction is expected only to produce CH_3NiOH or to restore the initial reactants, NiO + CH_4. ScO is not reactive with respect to methane at low and ambient temperatures. At elevated temperatures, the ScO + CH_4 reaction can proceed via a barrier of 22.4 kcal/mol to form a CH_3ScOH molecule with exothermicity of 9.8 kcal/mol. CH_3ScOH is not likely to decompose to the methyl radical and ScOH because this process is 58.9 kcal/mol endothermic.

Introduction

Methane is one of the world's abundant resources, and although it can be easily burned, CH_4 is not versatile for chemical synthesis. Utilization of methane to produce practical chemicals is one of the desirable goals of the current chemical industry.[1] Therefore, the activation of methane and its conversion to other organic species have attracted significant attention.[2−9] If the strong C−H bond in CH_4 can be cleaved using a catalyst, free methyl radicals formed are much more reactive and can recombine with other species to yield useful chemical products. Although catalytic processes usually occur in solution or in a solid state, an approach to understanding reaction mechanisms of methane with potential catalysts (such as transition metal oxides) can start from the study of these reactions in the gas phase. For such a study, ab initio and density functional calculations of potential energy surfaces (PES) represent an invaluable tool. Once the gas phase reaction mechanisms are understood by means of theoretical and experimental studies, a comparison can be made between the reactions in the gas and condensed phases, and the role of condensed phase effects can be better comprehended. Thus, the gas phase studies provide the first steps toward a more detailed understanding of the role of electronic structure in the more complex systems involved in condensed phase chemistry.

The activation of C−H and C−C bonds in small hydrocarbons by various transition metal oxide ions and bare metal cations in the gas phase has been investigated experimentally and theoretically by a number of groups.[10−18] For instance, Schröder and Schwarz have studied the reaction between FeO^+ and CH_4 and suggested HO−Fe^+−CH_3 as a key intermediate on the basis of experimentally determined isotope effects.[10] Schwarz's group has systematically examined[11] the efficiency and product branching ratio of the gas phase reactions of various transition metal oxide ions with methane and found that early transition metal oxide ions, ScO^+, TiO^+, VO^+, and CrO^+, do not react, while those of late transition metals, MnO^+, FeO^+, CoO^+, and NiO^+, react with methane. Yoshizawa and coworkers[18] have theoretically studied PES of the $FeO^+ + CH_4$, $MnO^+ + CH_4$, and $CoO^+ + CH_4$ reactions using density functional calculations and suggested that the methane−methanol conversion can occur by the following mechanism: $MO^+ + CH_4 \rightarrow OM^+(CH_4) \rightarrow$ TS1 $\rightarrow$ HO−M^+−$CH_3 \rightarrow$ TS2 $\rightarrow M^+(CH_3OH) \rightarrow M^+ + CH_3OH$, where M is a transition metal. Additionally, Yoshizawa et al.[18c] have investigated abstraction of methane's hydrogen atom by iron-oxo species FeO^{2+}, FeO^+, and FeO and concluded that the concerted reaction path leading to the HO−$Fe^{(n+)}$−CH_3 intermediates is energetically more favorable. These authors concluded that the experimentally observed reaction efficiency and methanol/methyl product branching ratio can be rationalized in terms of the calculated barrier heights at TS1 and TS2.

† Tamkang University.
‡ Academia Sinica.

10.1021/jp026414r CCC: $22.00
Published on Web 11/23/2002

Much less is known about the reaction mechanism of neutral metal oxides with methane. On the contrary to the reactions of transition metal oxide ions, for which experimental measurements can be performed using mass spectrometry techniques (for example, Fourier transform ion cyclotron resonance (FTICR) mass spectrometry[11]), the studies of neutral reactions require the use of other experimental methods, with spectroscopic monitoring of the reaction intermediates and products. One of such methods is the matrix isolation infrared or Fourier transform infrared (FTIR) spectroscopy, which was employed, for example, to investigate the reactions of neutral transition metals with H_2O[19] and CO_2[20] molecules and recently the Be + CH_4 reaction.[21] These methods may be used to study the reactivity of neutral transition metal oxides toward CH_4. In this view, theoretical calculations of PES can provide valuable information concerning the reaction mechanism and energetics and give a guidance for future experiments. Previously, Broclawik et al.[22] have used density functional calculations to study the activation of methane over PdO and found that the palladium oxide and CH_4 can form a weak complex bound by 3.3 kcal/mol. The insertion of PdO into the methane C−H bond was predicted to have a significant activation energy of 24.5 kcal/mol and to lead to the CH_3PdOH molecule, 29.5 kcal/mol below the reactants. Our recent G2M(MP2) calculations[23] showed the BeO + CH_4 reaction to proceed by barrierless formation of CH_4BeO, for which the complex formation energy (20.7 kcal/mol) is much higher than those for the methane complexes with neutral PdO and FeO (5.7 kcal/mol)[18] and comparable with the formation energies of the complexes with transition metal oxides FeO^+ (22.8 kcal/mol), MnO^+ (16.2 kcal/mol), CoO^+ (26.5 kcal/mol),[17] and FeS^+ (16.4 kcal/mol).[24] CH_4BeO can isomerize to a CH_3BeOH molecule (87.8 kcal/mol below BeO + CH_4) via transition state TS1, which lies 6.5 kcal/mol lower in energy than the reactants.[23] CH_3BeOH can dissociate without an exit barrier to BeOH + CH_3 (0.5 kcal/mol below the reactants) or rearrange through a high barrier at transition state TS2 (25.7 kcal/mol above BeO + CH_4) to a weakly bound CH_3OHBe complex. The overall BeO + CH_4 → CH_3OH + Be reaction was computed to be 11.4 kcal/mol endothermic and to have the highest barrier of 25.7 kcal/mol. However, the reaction route leading to the BeOH + CH_3 radical products either via the CH_3BeOH intermediate or by direct hydrogen abstraction is more feasible.[23]

The goal of the present paper is to study PES and mechanisms of reactions of neutral transition metal oxides with CH_4 in order to analyze the possibility of the methane → free methyl radical and methane → methanol conversion using MO. For this purpose, we considered the oxides of an early transition metal (Sc) and a late transition metal (Ni) and used the density functional theory (DFT) to calculate PES for the MO + CH_4 → M + CH_3OH and MO + CH_4 → MOH + CH_3 reactions. Because nickel oxide appeared to be reactive toward CH_4, we have also studied its heavier analogue, PdO.

Computational Details

As mentioned above, we have studied the lowest doublet PES for the ScO + CH_4 reaction as well as triplet and singlet surfaces for NiO/PdO + CH_4. For M = Sc, the first excited electronic states of the metal, ^4F ($3d^24s$), and of the oxide, $^2\Delta$, lie relatively high in energy, 32.9[25] and 43.0[26] kcal/mol above the ground state Sc(^2D) and ScO($^2\Sigma^+$), respectively; therefore, we investigated only the ground electronic state doublet PES. On the other hand, for Ni and Pd, the two lowest in energy triplet and singlet electronic states, PESs are quite close to each other and may interconvert during the reaction. Hence, we considered both triplet and singlet surfaces. For the ScO and NiO reactions, full geometry optimizations were run to locate all of the stationary points and transition states at the B3LYP/6-31G(d,p) level of theory.[27,28] We used spin-unrestricted B3LYP (UB3LYP) calculations for the doublet and triplet states. On the singlet NiO + CH_4 surface, both a reactant NiO($^1\Delta$) and a product Ni(^1D) have open shell wave functions. Therefore, for intermediates and transition states, we carried out calculations for open and closed shell singlet states using the UB3LYP and spin-restricted RB3LYP methods, respectively, and then compared their energies and chose the species with lower energies to obtain the PES for the lowest singlet state. In these cases, we carried out both RB3LYP and UB3LYP geometry optimizations. Harmonic vibrational frequencies were obtained at the same level of theory in order to characterize the stationary points as minima or first-order saddle points, to obtain zero-point vibration energy corrections (ZPE) and to generate force constant data needed for the intrinsic reaction coordinate (IRC) calculations. The IRC method[29] was used to track minimum energy paths from transition structures to the corresponding minima. A step size of 0.1 amu$^{1/2}$ bohr or larger was used in the IRC procedure. The relative energies of various species were then refined by single-point calculations at the B3LYP/6-31G(d,p) optimized geometries using the B3LYP method with the large 6-311+G(3df,2p) basis set, B3LYP/6-311+G(3df,2p)//B3LYP/6-31G(d,p). Unless otherwise mentioned, all relative energies for the ScO/CH_4 and NiO/CH_4 systems include ZPE corrections obtained at the B3LYP/6-31G(d,p) level.

For the reactions of the heavier transition metal oxide, PdO, we used basis sets in combination with effective core potential on the metal atoms. The smaller basis set I included the relativistic core potential (RECP) of Hay and Wadt[30] for Pd and double-ζ quality basis functions on both metal[30] and lighter O, C, and H atoms[31] augmented with polarization d functions for C and O, p functions for H, and f functions for Pd.[32] In basis set II, the RECP of Dolg et al. and the associated triple-ζ basis set[33] with addition of the f polarization functions[32] have been used for the metal, and Dunning's correlation consistent basis set cc-pVTZ[34] has been used for O, C, and H, while excluding f functions on O and C and d functions on H. Geometry optimization, normal mode analysis, and IRC calculations have been performed at the B3LYP/I level. The unscaled ZPEs calculated at the B3LYP/I level are included in our final energetics obtained by single-point calculations at the B3LYP/II level. It should be noted that similar basis sets were used by Cui, Musaev, and Morokuma[35] in their B3LYP calculations of methane activation by Pd, Pt, Pd_2, and Pt_2.

To assess the expected accuracy of our calculations, we recalculated the energies of various electronic states of metal atoms and their oxides using the coupled cluster[36] CCSD(T) method and multirefrence CASSCF[37] and MRCI[38] approaches with full valence active space and various basis sets. The calculations described here were performed employing the Gaussian 98[39] and MOLPRO 2000[40] programs.

Results and Discussion

Assessment of Computational Methods. The calculated singlet−triplet energy differences for M and MO (M = Ni, Pd) and the M−O bond strengths are shown in Table 1. The singlet−triplet energy gap for the Ni atom (between the ^3F ($3d^84s^2$) and ^1D ($3d^94s^1$) states), 9.7 kcal/mol in experiment,[25] is difficult to reproduce by single-reference-based ab initio methods. At the UCCSD(T)/6-311+G(3df) level, this energy is computed as 1.5

TABLE 1: Energy Differences between Low-Lying Electronic States for Ni, Pd, NiO, and PdO and Ni−O and Pd−O Bond Strengths in the Ground $^3\Sigma^-$ Electronic State of NiO and PdO (kcal/mol) Calculated at Different Levels of Theory

method	Ni, $^3F-^1D$	NiO, $^3\Sigma^- - ^1\Delta$	NiO, $^3\Sigma^- - ^1\Sigma^+$	Ni−O bond
B3LYP/6-31G(d)	19.5	10.5	35.1	81.8
B3LYP/6-311G(d)	18.4	14.9	35.9	70.0
B3LYP/6-311+G(3df)	3.0	10.6	33.9	83.9
CCSD/6-311G(d)	16.4	21.1	28.5	47.1
CCSD/6-311+G(3df)	5.1	26.7	28.1	68.7
CCSD(T)/6-311G(d)	9.5	29.9	15.1	64.2
CCSD(T)/6-311+G(3df)	1.5	35.8	16.7	87.2
CASSCF[a]/6-311+G(3df)	7.1	18.5	39.5	116.9
MRCI[a]/6-311+G(3df)	6.7	23.7	33.4	61.7 (78.9)[b]
MRCI+Q[a]/6-311+G(3df)	6.3	26.0	34.8	75.1 (89.9)[b]
experiment	9.7[c]	21.7[d]	41.5[d]	90.4[e]

method	Pd, $^1S-^3D$	PdO, $^3\Sigma^- - ^3\Pi$	PdO, $^3\Sigma^- - ^1\Sigma^+$	Pd−O bond
B3LYP/I	19.2	0.9	25.8	55.4
B3LYP/II	18.1	1.7	27.3	58.1
CCSD(T)/II	13.6	4.2	16.4	57.2
CASSCF[a]/II	5.1	1.7	16.1	20.4
MRCI[a]/II	17.3	2.4	17.1	35.1 (56.7)[b]
MRCI+Q[a]/II	18.0	3.3	18.0	48.6 (64.5)[b]
experiment	21.9[c]			66.2[f]

[a] Full valence active space calculations; the active space is (10,6) for Ni and Pd, (16,10) for NiO and PdO, and (6,4) for O. [b] In parentheses, bond strength computed using the supermolecule approach where the energy of M + O was calculated for the two atoms separated by 100 Å. [c] From ref 25. [d] From ref 41. [e] From ref 43. [f] From ref 52.

kcal/mol, while the UCCSD(T)/6-311G(d,p) calculations fortuitously give the $^3F-^1D$ energy gap very close to experiment. Density functional UB3LYP/6-311+G(3df) calculations result in 3.0 kcal/mol. Full valence active space CASSCF and MRCI/6-311+G(3df) calculations for the Ni atom result in 6.3−7.1 kcal/mol for the singlet−triplet energy difference, in reasonable agreement with the experimental value.

Various electronic states of NiO have been investigated both experimentally and theoretically.[41,42] According to photoelectron spectroscopic measurements by Wu and Wang,[41] the two lowest singlet states of nickel oxide are $^1\Delta$ and $^1\Sigma^+$, which, respectively, lie 21.7 and 41.5 kcal/mol above the ground $^3\Sigma^-$ state. As can be seen in Table 1, these values are not accurately reproduced even by sophisticated ab initio calculations. For instance, B3LYP calculations with various basis sets gave the $^3\Sigma^- - ^1\Delta$ and $^3\Sigma^- - ^1\Sigma^+$ energy differences as 10−15 and 34−36 kcal/mol and significantly underestimate the experimental results. The CCSD method overestimates the $^3\Sigma^- - ^1\Delta$ splitting by ∼5 kcal/mol but underestimates $^3\Sigma^- - ^1\Sigma^+$ by ∼13 kcal/mol. When triple excitations are included as perturbation, the agreement with experiment drastically worsens; at CCSD(T) levels, two singlet states switch their order and $^1\Sigma^+$ and $^1\Delta$ are calculated to lie 15−17 and 30−36 kcal/mol higher than the ground triplet state. Although the CASSCF calculations give the singlet−triplet energy gaps as 18.5 and 39.5 kcal/mol, close to experiment, the higher level MRCI/6-311+G(3df) approximation overestimates the $^1\Delta$ energy and underestimates $^1\Sigma^+$.

In experiment, the bond strength in the ground state nickel oxide is 90.4 kcal/mol.[43] The bond strength calculated at the CCSD(T)/6-311+G(3df) level with ZPE correction based on the experimental vibrational frequency is 87.2 kcal/mol, close to the MR-ACPF result by Bauschlicher and Maitze[44] (87.6 kcal/mol) and in reasonable agreement with experiment. B3LYP/6-311+G(3df) calculations give a slightly underestimated value of 83.9 kcal/mol, while CCSD(T) and B3LYP with the 6-311G(d) basis sets give the results more than 20 kcal/mol too low as compared to experiment.

The above comparisons and our earlier studies of the ScO + H_2,[45] NiO + H_2,[46] Sc + CO_2,[47] and Ti + CO_2[48] reactions, where we compared the accuracy of the B3LYP/6-311+G(3df,2p)//B3LYP/6-31G(d,p) method with those of CCSD(T) and multirefrence CASSCF and MRCI, show that the B3LYP approach is a reasonable compromise between the computational cost and the accuracy. While B3LYP provides less accurate results for the energy gaps between different electronic states of transition metals and their oxides than the multireference methods, it appears to be superior with respect to the much more costly CCSD(T) concerning the singlet−triplet energy splitting for M and MO and the heats and barriers of the MO + H_2 → M + H_2O and M + CO_2 → MO + CO reactions.

The ground state of the Pd atom has a closed shell ^1S electronic state (d^{10} electronic configuration), and the open shell ^3D (s^1d^9) state is 21.9 kcal/mol above.[25] B3LYP and MRCI results are in a good agreement with the experimental value giving the $^1S-^3D$ energy gap as 18−19 kcal/mol (Table 1), while the CCSD(T) and CASSCF methods significantly underestimate the experimental result. Because the experimental ground state of PdO is not known, there has been a continuing discussion among theorists what electronic state, $^3\Sigma^-$ or $^3\Pi$, is lower in energy for palladium oxide. In a CI calculation, Bauschlicher et al.[49] found that these states lie very close in energy, but because they used different CI expansions, they could not decide which is the lowest state. The MP2 and CISD methods predicted a $^3\Pi$ ground state,[50] but later, relativistic DFT calculations by Chung et al.[51] gave the $^3\Sigma^-$ energy as 16.4 kcal/mol lower than that of $^3\Pi$. More recent nonrelativistic B88-LYP calculations by Broclawik et al.[22] resulted in a very small (∼0.5 kcal/mol) energy difference with $^3\Pi$ being slightly more favorable. Our full valence MRCI calculations with addition of the Davidson correction for quadruple excitations (MRCI+Q) use the same CI expansion for both states and include most important relativistic effects via the use of RECP, so we expect that the computed $^3\Sigma^- - ^3\Pi$ energy gap of 3.3 kcal/mol is a reliable prediction. It should be noted that the B3LYP/II value is only 1.6 kcal/mol lower, and all other methods used in our calculations consistently give $^3\Sigma^-$ as the ground state lying 1−4 kcal/mol below $^3\Pi$.

The experimental dissociation energy of PdO to Pd(^1S) and O(^3P), 66.2 kcal/mol,[52] is best reproduced by the MRCI+Q/II approach using supermolecule calculations (see Table 1), which gives 64.5 kcal/mol. B3LYP, CCSD(T), and MRCI methods with basis set II underestimate the experimental value by 8−9 kcal/mol. Summarizing, the B3LYP/II method in most cases gives the results reasonably close to those obtained by much more expensive CCSD(T) and MRCI calculations, except for the singlet−triplet energy gap in PdO overestimated by ∼9 kcal/mol. Therefore, one should keep in mind that the B3LYP results for the early stages of the reaction of PdO may somewhat overestimate the energy difference between triplet and singlet structures.

ScO + CH_4 Reaction Mechanism. Relative energies of various compounds in the ScO + CH_4 reaction calculated at the B3LYP/6-31G(d,p) and B3LYP/6-311+G(3df,2p) levels of theory are listed in Table 2, while Table S1 of Supporting Information presents vibrational frequencies for various species. The energy diagram along the ScO + CH_4 reaction pathways computed at the B3LYP/6-311+G(3df,2p)//B3LYP/6-31G(d,p) level is shown in Figure 1, and the optimized geometric

TABLE 2: ZPE-Corrected Relative Energies (kcal/mol) of Various Compounds in the ScO + CH_4 Reaction Calculated at the B3LYP/6-31G(d,p) and B3LYP/6-311+G(3df,2p) Levels of Theory at B3LYP/6-31G(d,p) Optimized Geometries

species	B3LYP/ 6-31G(d,p)	B3LYP/ 6-311+G(3df,2p)
$ScO(^2\Sigma^+) + CH_4$	0	0
TS1	21.92	22.39
CH_3ScOH	−6.42	−9.75
$ScOH + CH_3$	52.06	49.16
TS2	78.20	76.04
$ScCH_3OH$	61.81	60.57
$Sc(^2D) + CH_3OH$	77.07	72.92

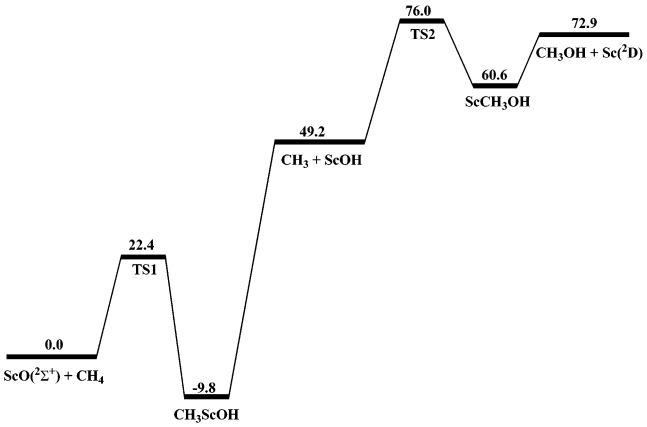

Figure 1. Potential energy diagram for the ScO + CH_4 → ScOH + CH_3 → Sc + CH_3OH reactions calculated at the B3LYP/6-311+G(3df,2p)//B3LYP/6-31G(d,p) + ZPE(B3LYP/6-31G(d,p)) level.

structures of various reactants, intermediates, transition states, and products are collected in Figure 2. The calculations show that scandium oxide is unable to form a stable molecular complex with methane. Instead, the reaction proceeds by insertion of ScO into the C−H bond producing the CH_3ScOH intermediate via TS1 (see Figures 1 and 2). In this view, the mechanism of the ScO + CH_4 reaction is similar to that of ScO + H_2.[45] For the latter, also no stable $OScH_2$ molecular complex exists and the insertion of ScO into the H−H bond results in the HScOH molecule. The B3LYP/6-311+G(3df,2p)//B3LYP/6-31G(d,p) calculated exothermicity of the ScO + CH_4 → CH_3ScOH reaction step is 9.7 kcal/mol, and the barrier at TS1 is 22.4 kcal/mol. The IRC calculations at the B3LYP/6-31G(d,p) level of theory have confirmed that transition state TS1 connects the CH_4 + ScO reactants with CH_3ScOH. The geometries of the ScOH fragments in the CH_3ScOH and HScOH molecules are very similar, so that the substitution of H by the methyl group plays a minor role for the structure. On the other hand, the binding energy of CH_3ScOH relative to ScO + CH_4 (9.7 kcal/mol) is notably lower than that of HScOH with respect to ScO + H_2 (14.2 kcal/mol at the same B3LYP/6-311+G(3df,2p)//B3LYP/6-31G(d,p) level of theory[45]). Apparently, the Sc−C bond in CH_3ScOH is slightly weaker than the Sc−H bond in HScOH. The decrease of the reaction exothermicity when ScO reacts with methane instead of molecular hydrogen is also reflected by an increase of the reaction barrier from 13.7 kcal/mol for ScO + H_2 to 22.4 kcal/mol for the ScO + CH_4 reaction.

In the ScO + H_2 reaction, the HScOH intermediate can undergo a 1,2-H shift from Sc to H with formation of the Sc−OH_2 molecular complex via a high barrier of ∼57 kcal/mol.[45] This appeared not to be the case for the CH_3ScOH molecule. Despite a careful search, we failed to locate a transition state

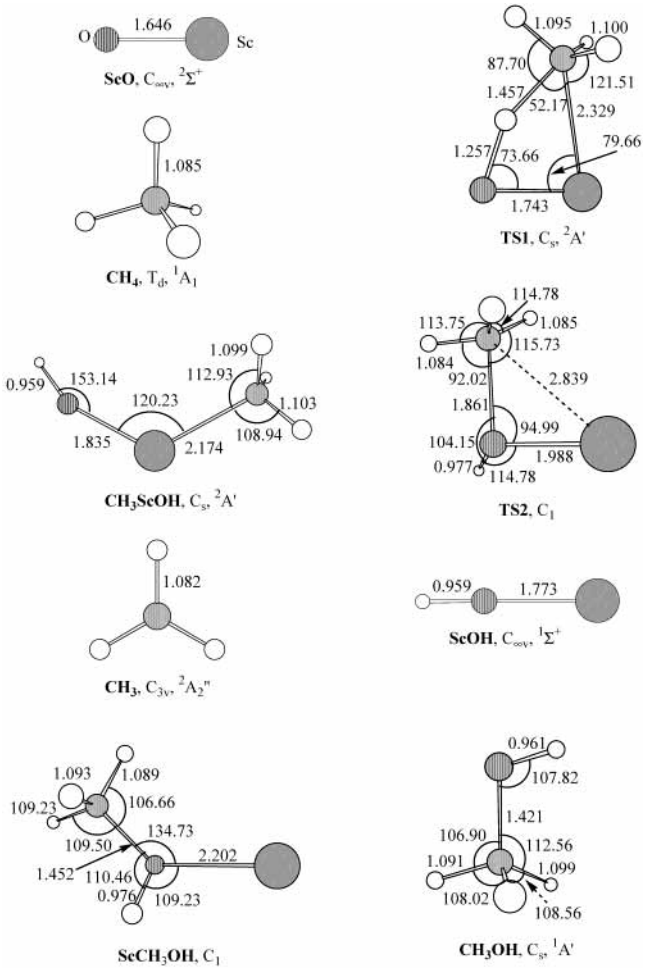

Figure 2. Geometries of the reactants, products, intermediates, and transition states of the ScO + CH_4 → ScOH + CH_3 → Sc + CH_3OH reactions, optimized at the B3LYP/6-31G(d,p) level. (Bond lengths are in Å, and bond angles are in degrees.)

for the methyl group 1,2-migration leading to the Sc−methanol complex. The saddle point optimization instead leads to the CH_3 + ScOH dissociation products indicating that CH_3ScOH rather decomposes with the Sc−C bond cleavage than isomerizes to $ScCH_3OH$. The bond cleavage takes place without an exit barrier. The calculated endothermicity of the ScO + CH_4 → ScOH + CH_3 reaction is high, 49.2 kcal/mol, and this reaction is unlikely to occur. At elevated temperatures, when the 22.4 kcal/mol barrier at TS1 can be overcome, the ScO + CH_4 reaction can produce CH_3ScOH. At higher temperature, the latter would rather dissociate to ScO + CH_4 via the barrier of 32.1 kcal/mol than to ScOH + CH_3 with an activation energy of 58.9 kcal/mol.

The ScOH + CH_3 reaction can occur by two different mechanisms. If methyl radical attacks ScOH from the Sc side, CH_3ScOH is produced without an entrance barrier and with high exothermicity. This intermediate can further easily decompose to ScO + CH_4 because transition state TS1 lies 26.8 kcal/mol below the ScOH + CH_3 reactants. Another pathway leading to the ScO + CH_4 products may be a direct abstraction of the hydrogen atom from ScOH by CH_3, but we do not consider this possibility here since it should be less favorable than the barrierless and 58.9 kcal/mol exothermic formation of CH_3ScOH at the initial reaction step. On the other hand, CH_3 can attack ScOH toward the middle oxygen atom. In this case, the $ScCH_3OH$ complex of the Sc atom with methanol can be produced via transition state TS2. The ScOH + CH_3 →

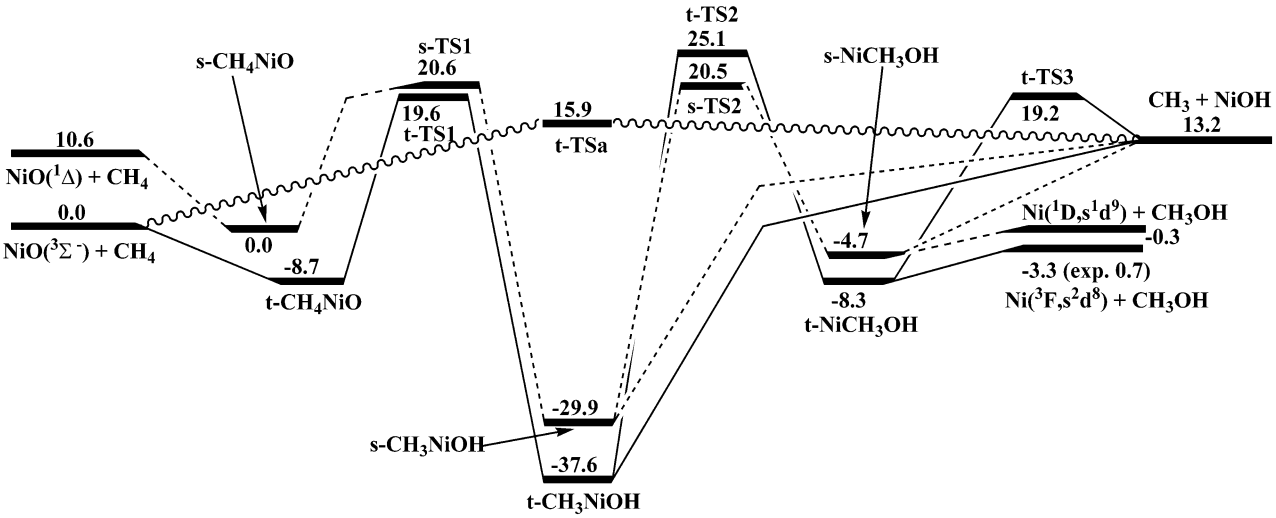

Figure 3. Potential energy diagram for the NiO + CH_4 → Ni + CH_3OH reaction calculated at the B3LYP/6-311+G(3df,2p)//B3LYP/6-31G(d,p) + ZPE(B3LYP/6-31G(d,p)) level.

$ScCH_3OH$ reaction is calculated to be 11.4 kcal/mol endothermic and exhibits a barrier of 26.9 kcal/mol. In the transition state TS2, the forming C−O bond length is 1.861 Å, 0.409 Å longer than that in the $ScCH_3OH$ complex, and the Sc−O bond lengthens from 1.773 Å in ScOH to 1.988 Å in TS2 and then to 2.202 Å in the product. The ScOH fragment, linear in the isolated molecule, bends in the transition state where the ScOH angle is 114.78°, which is close to 109.23° in $ScCH_3OH$. Therefore, TS2 is a rather late transition state, in line with the fact that the reaction is endothermic. The B3LYP/6-31G(d,p) IRC calculations confirmed that the first-order saddle point TS2 connects CH_3 + ScOH with $ScCH_3OH$. The complex of scandium atom with methanol is bound by 12.4 kcal/mol relative to CH_3OH + Sc, and its decomposition can take place without an exit barrier. The total endothermicity of the ScOH + CH_3 → TS2 → $ScCH_3OH$ → Sc + CH_3OH reaction and the highest barrier on the reaction pathway are computed as 23.8 and 26.9 kcal/mol, respectively. These values render the Sc + CH_3OH product channel in the ScOH + CH_3 reaction much less likely than the ScO + CH_4 channel.

It should be noted that the B3LYP/6-311+G(3df,2p)//B3LYP/6-31G(d,p) calculated relative energy of Sc + CH_3OH is 72.9 kcal/mol higher than that of ScO + CH_4, which is very close to the experimental value of 72.0 kcal/mol obtained based on the experimental bond strength in ScO, 161.7 kcal/mol,[53] and heats of formation of methane, methanol, and O.[26]

NiO + CH_4 Reaction Mechanism. *Triplet PES.* As seen in Figures 3 and 4, at the first step of the NiO($^3\Sigma^-$) + CH_4 reaction in triplet electronic state, the CH_4 molecule can be attached without a barrier to the Ni atom of NiO($^3\Sigma^-$) to form a molecular complex t-CH_4NiO (here and below prefixes "t" and "s" indicate triplet and singlet states, respectively) bound by 8.7 kcal/mol relative to the reactants (see Tables 3 and S2 of Supporting Information for relative energies and vibrational frequencies, respectively). The complex has no symmetry, and Ni is oriented toward two hydrogens of methane, for which the C−H bonds are slightly stretched to 1.120 Å (ca. with 1.085 Å in the free CH_4 molecule). The CNiO fragment in t-CH_4NiO is nearly linear, with the angle of 169.80°. The complex formation energy of NiO($^3\Sigma^-$) with methane is significantly higher than that with molecular hydrogen, 3.7 kcal/mol at the same level of theory.[46] At the next reaction step, NiO can insert into the C−H bond producing a t-CH_3NiOH intermediate via t-TS1. The calculated exothermicity of the t-CH_4NiO → t-CH_3NiOH reaction step is about 28.9 kcal/mol, and the barrier is 28.3 and 19.6 kcal/mol relative to t-CH_4NiO and NiO($^3\Sigma^-$) + CH_4, respectively. IRC calculations have confirmed the connection between t-CH_4NiO and t-CH_3NiOH through transition state t-TS1. The geometry of the NiOH fragment in t-CH_3NiOH is similar to that in the HNiOH molecule.[46] On the other hand, the energy of t-HNiOH relative to NiO($^3\Sigma^-$) + H_2, −44.8 kcal/mol, is ∼7 kcal/mol lower than the energy of t-CH_3NiOH with respect to NiO($^3\Sigma^-$) + CH_4, −37.6 kcal/mol, indicating that the Ni−C bond is weaker than Ni−H. Interestingly, the barriers for the NiO($^3\Sigma^-$) insertion into the C−H bond of methane and H−H bond of H_2 are very close, ∼19 kcal/mol relative to the reactants.

From the t-CH_3NiOH intermediate, the reaction can proceed by the 1,2-methyl group migration via transition state t-TS2 to t-$NiCH_3OH$, a complex between the Ni atom and the methanol. The Ni−C bond (2.290 Å) in t-TS2 becomes weaker, and a new C−O bond (1.861 Å) starts to form, while the Ni−O bond stretches from 1.741 to 1.847 Å. The transition state exhibits a rather late character, which is in accord with the fact that this reaction step is 29.3 kcal/mol endothermic. The barrier at t-TS2 is calculated to be high, 62.7 and 25.1 kcal/mol with respect to t-CH_3NiOH and the initial reactants, respectively. The B3LYP/6-31G(d,p) IRC calculations confirmed that the first-order saddle point t-TS2 connects the t-CH_3NiOH and t-$NiCH_3OH$ intermediates. t-$NiCH_3OH$, where the Ni atom is coordinated toward the O atom of methanol, is a rather weak complex, which decomposes to Ni(^{3}F) and CH_3OH with the energy loss of 5.0 kcal/mol and without an exit barrier. Overall, the NiO($^3\Sigma^-$) + CH_4 → Ni(^{3}F) + CH_3OH reaction is calculated to be 3.3 kcal/mol exothermic, while according to the experimental data it is 0.7 kcal/mol endothermic.[26] Nevertheless, the deviation between the experimental and the B3LYP/6-311+G(3df,2p)//B3LYP/6-31G(d,p) calculated ΔH_r is not large. Interestingly, the NiO($^3\Sigma^-$) + H_2 → Ni(^{3}F) + H_2O reaction is much more exothermic, ∼27 kcal/mol,[46] reflecting a stronger O−H bond in water as compared to O−C in CH_3OH.

Another possible product channel of the NiO($^3\Sigma^-$) + CH_4 reaction is CH_3 + NiOH(^{2}A″). The radical products can be formed by a direct abstraction of an H atom of CH_4 by the oxygen atom of NiO via transition state t-TSa. The transition state exhibits a typical geometry for a hydrogen abstraction TS, with a nearly linear (176.76°) C−H−O fragment. The breaking C−H bond is lengthened from 1.085 to 1.419 Å and the forming O−H bond, 1.121 Å, is only ∼0.15 Å longer than that in the

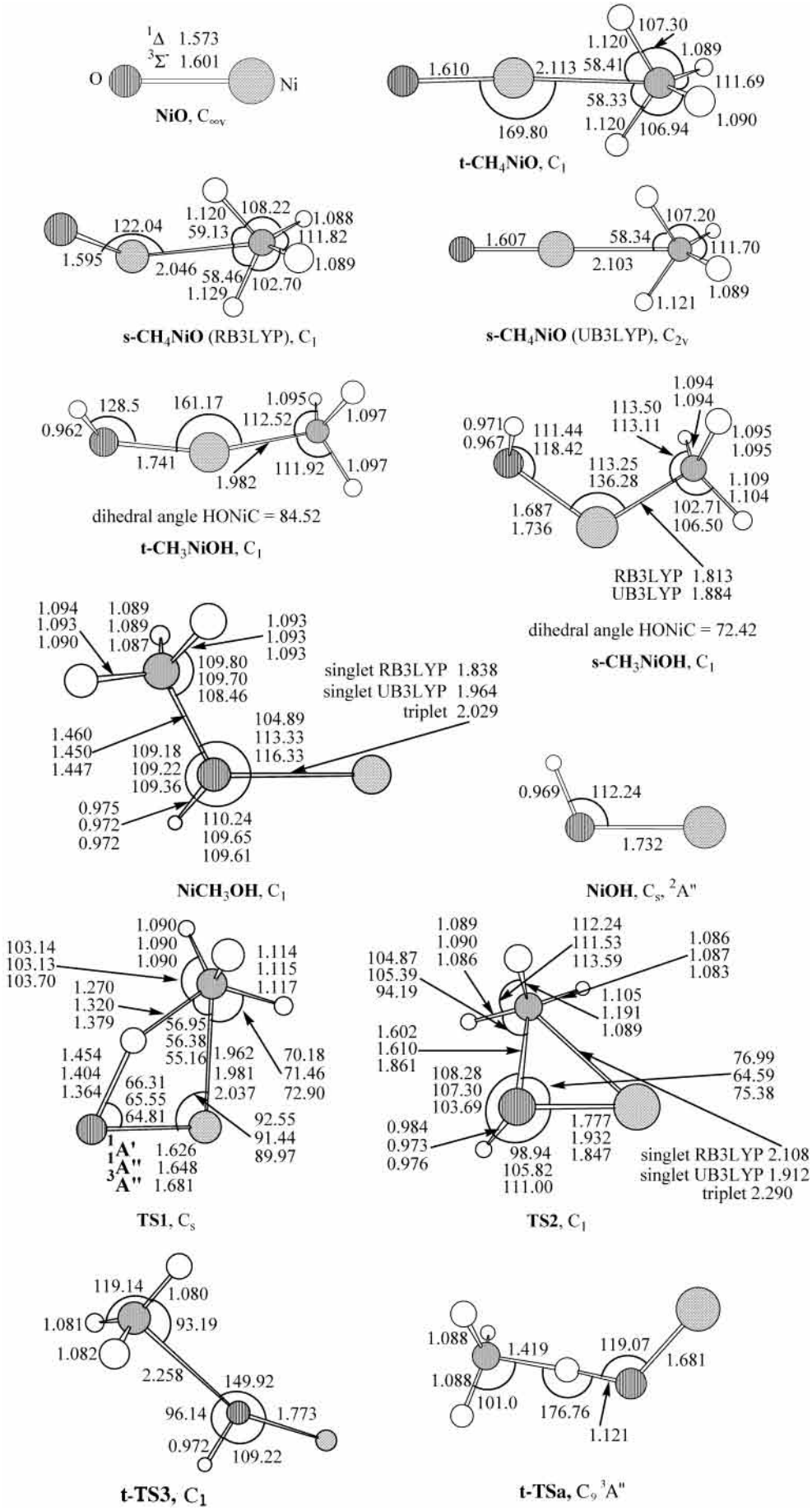

Figure 4. Geometries of the reactants, products, intermediates, and transition states of the NiO + CH_4 → Ni + CH_3OH reaction, optimized at the B3LYP/6-31G(d,p) level. (Bond lengths are in Å, and bond angles are in degrees.)

TABLE 3: ZPE-Corrected Relative Energies (kcal/mol) of Various Compounds in the NiO + CH_4 Reaction Calculated at the B3LYP/6-31G(d,p) and B3LYP/6-311+G(3df,2p) Levels of Theory at B3LYP/6-31G(d,p) Optimized Geometries

species	B3LYP/ 6-31G(d,p)	B3LYP/ 6-311+G(3df,2p)
$NiO(^3\Sigma^-) + CH_4$	0	0
t-CH_4NiO	−17.65	−8.70
t-TS1	8.34	19.60
t-CH_3NiOH	−54.36	−37.60
t-TS2	19.52	25.10
t-$NiCH_3OH$	−7.01	−8.28
$Ni(^3F) + CH_3OH$	1.73	−3.30
t-TS3	20.02	19.23
t-TSa	19.62	15.91
$NiOH(^2A'') + CH_3$	15.67	13.18
$NiO(^1\Delta) + CH_4$	10.53	10.61
	s-CH_4NiO	
RB3LYP	9.34	22.80
UB3LYP, $\langle S^2\rangle = 1.001$	−11.79	0.00
	s-TS1	
RB3LYP	14.48	23.74
UB3LYP, $\langle S^2\rangle = 0.629$	10.95	20.64
	s-CH_3NiOH	
RB3LYP	−35.13	−27.65
UB3LYP, $\langle S^2\rangle = 0.832$	−42.01	−29.88
	s-TS2	
RB3LYP	36.38	21.29
UB3LYP, $\langle S^2\rangle = 0.843$	23.57	20.48
	s-$NiCH_3OH$	
RB3LYP	27.94	−4.71
UB3LYP, $\langle S^2\rangle = 1.007$	7.53	−0.90
$Ni(^1D) + CH_3OH$	21.23	−0.31

NiOH radical. Thus, t-TSa has a late character, in line with the fact that the $NiO(^3\Sigma^-) + CH_4 \rightarrow CH_3 + NiOH$ reaction is computed to be 13.2 kcal/mol endothermic. The calculated barrier at t-TSa is 15.9 kcal/mol relative to the reactants but only 2.7 kcal/mol with respect to the products. The CH_3 + NiOH products can be also formed through the Ni−C bond cleavage in the t-CH_3NiOH intermediate. The t-$CH_3NiOH \rightarrow CH_3$ + NiOH reaction is 50.8 kcal/mol endothermic and takes place without an exit barrier; a transition state search for the Ni−C bond rupture in the t-CH_3NiOH molecule led to the radical products. On the other hand, the t-$NiCH_3OH$ complex can also dissociate to NiOH + CH_3 by a cleavage of the C−O bond. This process exhibits an exit barrier with transition state t-TS3 lying 19.2 and 6.0 kcal/mol above $NiO(^1\Delta) + CH_4$ and NiOH + CH_3, respectively. The transition state shows a late character with the breaking C−O bond of 2.258 Å, and the NiOH and CH_3 fragments have the geometries very close to those in the separated radicals.

Singlet PES. The singlet reaction pathway is similar to the triplet pathway, but the energies differ. At the B3LYP/6-311+G(3df,2p)//B3LYP/6-31G(d,p) level, singlet $NiO(^1\Delta)$ lies 10.6 kcal/mol above the ground $^3\Sigma^-$ triplet state, so that the experimental energy gap between the two states, 21.7 kcal/mol, is underestimated by two times. All intermediates and transition states of the $NiO(^1\Delta) + CH_4$ reaction, except the s-$NiCH_3OH$ complex, have open shell wave functions in their lowest singlet states, i.e., their UB3LYP/6-311+G(3df,2p)//UB3LYP/6-31G(d,p) energies are lower than the RB3LYP/6-311+G(3df,2p)//RB3LYP/6-31G(d,p) energies (Table 3). The $\langle S^2\rangle$ values at the UB3LYP level are typically in the range of 0.63−1.00 before annihilation of higher spin contributions in the wave functions but decrease to 0.02−0.05 after the annihilation, which indicates a significant spin contamination of the open shell singlet wave function by the triplet state. A removal of the spin contamination would result in an increase of the triplet−singlet energy gap for NiO, Ni, and various intermediates and transition states.

At the initial reaction step, $NiO(^1\Delta)$ and CH_4 form the s-CH_4NiO complex stabilized by 10.6 kcal/mol relative to the reactants. Thus, the complex formation energy in the singlet state is 1.9 kcal/mol higher than in the triplet state. This is also the case for the molecular complex of nickel oxide with H_2 for which the complex formation energies are 6.1 and 3.7 kcal/mol in singlet and triplet, respectively.[46] Still, s-CH_4NiO lies 8.7 kcal/mol above t-CH_4NiO. The major difference in the t-CH_4NiO and s-CH_4NiO geometries is seen for the CNiO angle, 169.80° for triplet vs 180° for singlet, i.e., the latter has a C_{2v} symmetric structure with the linear CNiO fragment. The energy barrier for NiO insertion into the C−H bond separating s-CH_4NiO from s-CH_3NiOH is 20.6 kcal/mol and s-TS1 is only 1.0 kcal/mol higher in energy than t-TS1. s-TS1 shows a somewhat earlier character than the triplet transition state, with a shorter breaking C−H bond (1.320 vs 1.379 Å in t-TS1) and a longer forming O−H bond (1.404 vs 1.364 Å). The s-CH_3NiOH molecule produced after the insertion is 7.7 kcal/mol higher in energy than the ground state triplet t-CH_3NiOH and lies 29.9 and 40.5 below the triplet and singlet reactants, respectively. Optimized geometric parameters of CH_3NiOH in the triplet and singlet states significantly differ for the CNiO (161.17 and 136.28°) and NiOH (128.50 and 118.42°) angles as well as for the C−Ni bond length, ∼0.1 Å shorter in the singlet than in the triplet state. From s-CH_3NiOH, the reaction can proceed by the C−Ni bond cleavage to form the radical CH_3 + NiOH products without an exit barrier. On the other hand, the methyl group migration from Ni to O leads to the s-$NiCH_3OH$ complex via s-TS2. The energy of s-TS2, 20.5 kcal/mol relative to $NiO(^3\Sigma^-) + CH_4$, is 4.6 kcal/mol lower than that of t-TS2. In the singlet transition state, both Ni−C and C−O distances are much (by 0.25−0.4 Å) shorter than those in t-TS2 but the Ni−O distance is ∼0.09 Å longer. The s-$NiCH_3OH$ complex, 3.6 kcal/mol higher in energy than t-$NiCH_3OH$, is stabilized by 4.4 kcal/mol with respect to $Ni(^1D) + CH_3OH$ and can decompose to them without an exit barrier. It should be noted that the B3LYP/6-311+G(3df,2p) calculations underestimate the experimental $^1D-^3F$ energy gap for the Ni atom by 6.7 kcal/mol.

Overall Reaction Mechanism. Similar to the NiO + H_2 reaction,[46] the reaction of the nickel oxide with methane may involve both triplet and singlet PESs. The minimal energy reaction pathway starts from the formation of the t-CH_4NiO complex from $NiO(^3\Sigma^-)$ and CH_4. Next, the t-CH_3NiOH intermediate is produced via t-TS1 overcoming a barrier of 19.6 kcal/mol with respect to the reactants. For the NiO + H_2 reaction,[46] the minimal energy pathway goes through the singlet transition state s-TS1, which is ∼6 kcal/mol lower than t-TS1, and thus involves a singlet−triplet intersystem crossing. This is not the case for NiO + CH_4; s-TS1 is slightly higher in energy than the triplet transition state for NiO insertion into the C−H bond. t-CH_3NiOH decomposes to CH_3 + NiOH or undergoes a 1,2-CH_3 migration to form a molecular complex between the Ni atom and the methanol. If a singlet−triplet intersystem crossing takes place along the reaction path, the barrier for this reaction step can be lowered from 25.1 kcal/mol (relative to the initial reactants) at t-TS2 to 20.5 kcal/mol at s-TS2. After the barrier is cleared on the singlet state PES, another intersystem crossing can lead to the t-$NiCH_3OH$ complex, 3.6 kcal/mol lower in energy than s-$NiCH_3OH$. Finally, the complex decomposes into the triplet $Ni(^3F) + CH_3OH$ products. Earlier,[46] we showed that the intersystem crossing indeed takes place

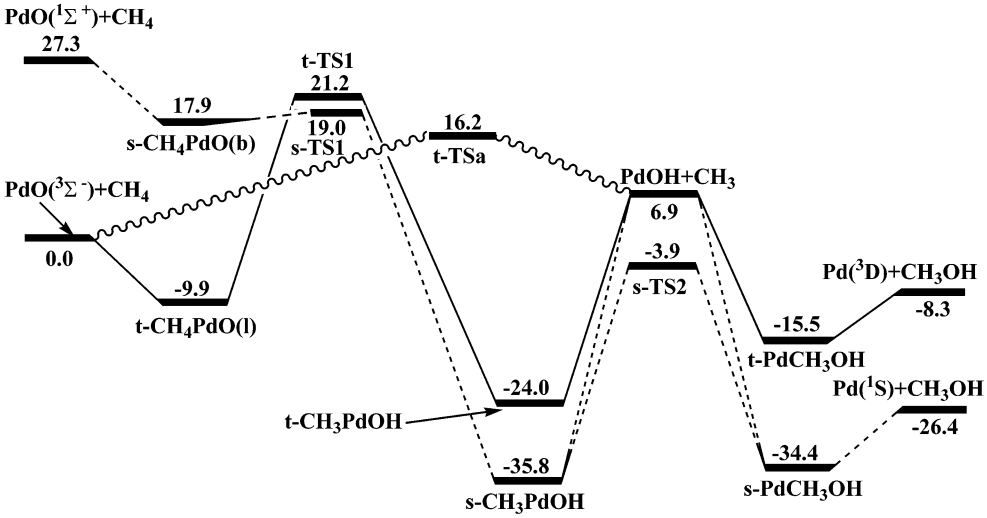

Figure 5. Potential energy diagram for the PdO + CH_4 → Pd + CH_3OH reaction calculated at the B3LYP/II//I + ZPE(B3LYP/I) level.

between singlet and triplet PES of the HNiOH system in the vicinity of the transition state for the 1,2-H shift from Ni to O. The spin−orbit coupling between the singlet and the triplet states at a representative point on the crossing seam was computed as 27 cm^{-1}.[46] From the potential energy diagram for the CH_3NiOH system (Figure 3), one can expect that the singlet−triplet intersection can also occur in the vicinity of s- and t-TS2.

The barriers on the NiO($^3\Sigma^-$) + CH_4 → Ni(^{3}F) + CH_3OH reaction pathway are calculated as ∼20 kcal/mol with respect to the reactants. This means that at elevated temperatures in the gas phase nickel oxide might directly transform methane to methanol. However, according to the computed energies, the reaction mechanism leading to CH_3OH is not favorable. The direct hydrogen abstraction leading to the CH_3 + NiOH is preferable since the barrier for this mechanism is lower, 15.9 kcal/mol. The radical products can be also formed by the NiO($^3\Sigma^-$) + CH_4 → t-CH_4NiO → t-TS1 → t-CH_3NiOH → CH_3 + NiOH pathway. Once the t-CH_3NiOH intermediate is produced, it is more likely to decompose to CH_3 + NiOH with the activation energy of 50.8 kcal/mol than to rearrange into the t-NiCH_3OH complex via the barrier of 58.1 kcal/mol and singlet−triplet intersystem crossing or via the barrier of 62.7 kcal/mol in the triplet state. Hence, while NiO is able to assist the methane activation at elevated temperatures, the methanol/methyl product branching ratio is expected to be low. At low and ambient temperatures, the NiO($^3\Sigma^-$) + CH_4 reaction can produce only the t-CH_4NiO molecular complex bound by 8.7 kcal/mol.

PdO + CH_4 Reaction Mechanism. Relative energies of various species in the PdO + CH_4 reaction calculated at the B3LYP/I and B3LYP/II levels of theory are presented in Table 4, while Table S3 of Supporting Information lists their vibrational frequencies. The energy diagram along the PdO + CH_4 reaction pathways computed at the B3LYP/II//B3LYP/I level is shown in Figure 5, and the optimized geometric structures of various reactants, intermediates, transition states, and products are depicted in Figure 6. Similarly to Broclawik et al.,[22] we found two types of complexes of palladium oxide with methane corresponding to collinear and bridging adsorption of CH_4. In the triplet electronic state, only the collinear t-CH_4PdO(l) complex is a local minimum. It has C_{2v} symmetry with two H atoms of methane oriented toward the Pd atom (see Figure 6). The minima were located in two triplet states, $^3B_1$ and $^3A_2$, where the latter lies 4.7 kcal/mol lower in energy than the former and is stabilized by 9.9 kcal/mol with respect to the reactants, PdO($^3\Sigma^-$) + CH_4. In t-CH_4PdO(l), $^3A_2$, the C−H bonds directed to Pd are slightly stretched (to 1.111 Å) and the Pd−H distances are relatively short, 2.129 Å. The Pd−O bond length is nearly unchanged as compared to the free PdO($^3\Sigma^-$) molecule. The complex formation energy computed at the B3LYP/II level is significantly higher than 3.3 kcal/mol obtained by Broclawik et al. at the B88-LYP level[22] and is comparable with that for t-CH_4NiO. In the singlet electronic state, the s-CH_4PdO(b) complex in C_s symmetry corresponds to bridging adsorption of methane and no collinear complex was found as a local minimum. One of the CH_4 hydrogens interacts with O and another with Pd with O−H and Pd−H distances of 2.218 and 2.048 Å, respectively. s-CH_4PdO(b) lies 9.4 kcal/mol below the PdO($^1\Sigma^+$) + CH_4 reactants, so the complex formation energy for singlet is similar to that for triplet.

Both triplet and singlet reactions proceed from the complexes by insertion of the palladium oxide into a C−H bond via TS1. In the triplet state, the barrier is high, 31.1 and 21.2 kcal/mol relative to t-CH_4PdO(l) and PdO($^3\Sigma^-$) + CH_4, respectively. On the other hand, in the singlet state, the calculated barrier is only 1.1 kcal/mol with respect to s-CH_4PdO(b) and s-TS1 lies 19.0 kcal/mol above PdO($^3\Sigma^-$) + CH_4 and 2.2 kcal/mol below t-TS1. s-TS1 has a much earlier character than t-TS1, which is indicated by a shorter length for the breaking C−H bond (1.219 Å in the former vs 1.400 Å in the latter) and a longer length for the forming O−H bond (1.480 Å vs 1.244 Å). Because the energies

TABLE 4: ZPE-Corrected Relative Energies (kcal/mol) of Various Compounds in the PdO + CH_4 Reaction Calculated at the B3LYP/I and B3LYP/II Levels of Theory at B3LYP/I Optimized Geometries

species	B3LYP/I	B3LYP/II
PdO($^3\Sigma^-$) + CH_4	0	0
t-CH_4PdO(l), $^3A_2$	−8.79	−9.85
t-CH_4PdO(l), $^3B_1$	−5.11	−5.14
t-TS1	20.27	21.17
t-CH_3PdOH	−21.04	−24.02
t-TSa	14.65	16.15
PdOH($^2A''$) + CH_3($^2A_2''$)	7.12	6.93
t-PdCH_3OH	−17.06	−15.45
Pd(^{3}D) + CH_3OH	−8.91	−8.27
PdO($^1\Sigma^+$) + CH_4	25.82	27.31
s-CH_4PdO(b)	17.67	17.86
s-TS1	18.69	19.02
s-CH_3PdOH	−35.03	−35.81
s-TS2	−4.69	−3.91
s-PdCH_3OH	−35.80	−34.36
Pd(^{1}S) + CH_3OH	−28.15	−26.39

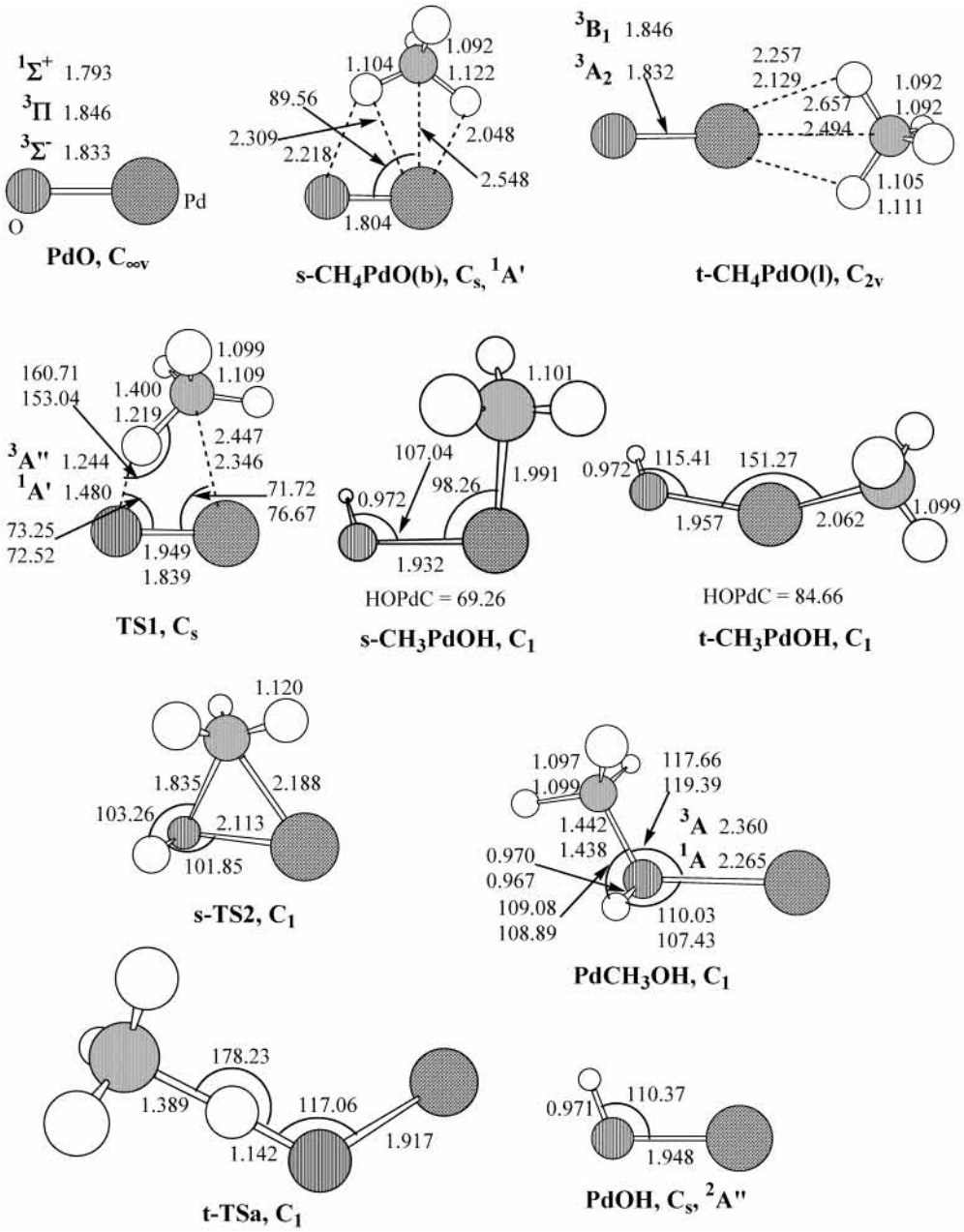

Figure 6. Geometries of the reactants, products, intermediates, and transition states of the PdO + CH_4 → Pd + CH_3OH reaction, optimized at the B3LYP/I level. (Bond lengths are in Å, and bond angles are in degrees.)

of t- and s-TS1 are close, one can expect that the singlet and triplet PES can cross in a vicinity of this transition state. Indeed, calculations of a triplet state at the s-TS1 geometry show that the singlet ^{1}A′ and triplet ^{3}A″ energies are nearly identical and differ only by 1 and 50 cm^{-1} at the B3LYP/I and B3LYP/II levels, respectively. Thus, the singlet−triplet intersystem crossing takes place at s-TS1. The ground electronic state reaction, PdO($^3\Sigma^-$) + CH_4, proceeds on the triplet PES before reaching the s-TS1 structure where the system can switch its multiplicity and continue on the singlet PES. Because s-TS1 develops earlier than t-TS1, the higher barrier in the triplet state at t-TS1 does not have to be overcome.

The insertion of PdO into a C−H bond of methane leads to the formation of a CH_3PdOH molecule. Its structures in the singlet and triplet states are quite different. s-CH_3PdOH has shorter Pd−O and Pd−C bond lengths, 1.932 and 1.991 Å, respectively, vs 1.957 and 2.062 Å in t-CH_3PdOH, and much smaller CPdO and PdOH angles, 98.26 and 107.04°, respectively, vs 151.27 and 115.41°. The singlet CH_3PdOH resides 35.8 kcal/mol lower in energy than the PdO($^3\Sigma^-$) + CH_4 reactants and is 13.8 kcal/mol more stable than t-CH_3PdOH. In the singlet state, the reaction can continue by 1,2-migration of the methyl group from Pd to O via s-TS2. In the transition state, the Pd−C and Pd−O bonds are stretched as compared to those in s-CH_3PdOH and a new Pd−O bond (1.835 Å) starts to form. The calculated barrier for the 1,2-CH_3 shift is 31.9 kcal/mol, but s-TS2 lies 3.9 kcal/mol below the initial reactants. Despite a careful search, we were not able to locate a corresponding t-TS2 in the triplet state. The saddle point search resulted in dissociation of the triplet molecule to PdOH(^{2}A″) and methyl radical indicating that CH_3 splitting is preferable as compared to its migration. After the barrier at s-TS2 is cleared, a s-PdCH_3OH complex between Pd atom and methanol is produced. The complex lies 34.4 kcal/mol lower in energy than the reactants and is stabilized by 8.0 kcal/mol with respect to Pd(^{1}S) + CH_3OH. A triplet t-PdCH_3OH complex can also exist,

although it is 19.9 kcal/mol less stable than s-PdCH$_3$OH. The complex formation energy of Pd(^{3}D) with methanol is 7.2 kcal/mol. t-PdCH$_3$OH can be produced without a barrier not only from Pd(^{3}D) + CH$_3$OH but also from PdOH and CH$_3$.

The overall exothermicity of the PdO($^3\Sigma^-$) + CH$_4$ → Pd(^{1}S) + CH$_3$OH reaction is calculated as 26.4 kcal/mol at the B3LYP/II//B3LYP/I level. Taking the experimental bond strength for PdO (66.2 kcal/mol[52]) and heats of formation of CH$_4$, CH$_3$OH, and O,[26] the experimental reaction heat is −23.5 kcal/mol, so our calculated result agrees with the experimental ΔH_r within 3 kcal/mol margins. The minimal energy pathway for methane conversion to methanol using palladium oxide involves both triplet and singlet PES and can be described as follows: PdO($^3\Sigma^-$) + CH$_4$ → t-CH$_4$PdOH(l) → s-TS1 → s-CH$_3$PdOH → s-TS2 → s-PdCH$_3$OH → Pd(^{1}S) + CH$_3$OH. Here, the reaction starts on the triplet surface, undergoes triplet−singlet intersystem crossing near s-TS1, and then continues in the singlet electronic state. Because Pd is a heavy element, the triplet-to-singlet conversion at the intersection point of PES is expected to be efficient. The PdO($^3\Sigma^-$) + CH$_4$ → Pd(^{1}S) + CH$_3$OH reaction is another example of the two state reactivity concept, which was recently discussed in detail by Schröder, Shaik, and Schwarz.[17,54]

The alternative channel for the PdO($^3\Sigma^-$) + CH$_4$ reaction is abstraction of a hydrogen atom to produce PdOH(^{2}A″) and CH$_3$. This channel is computed to be 6.9 kcal/mol endothermic and proceeds via transition state t-TSa with a barrier of 16.2 kcal/mol. In accord with the reaction endothermicity, t-TSa exhibits a rather late character; the forming Pd−O bond is 18% longer than that in isolated PdOH, while the breaking C−H bond is 27% longer than the bond in methane. The two channels, hydrogen abstraction, PdO($^3\Sigma^-$) + CH$_4$ → t-TSa → PdOH + CH$_3$, and PdO($^3\Sigma^-$) + CH$_4$ → t-CH$_4$PdOH(l) → s-TS1 → s-CH$_3$PdOH → s-TS2 → s-PdCH$_3$OH → Pd(^{1}S) + CH$_3$OH, are expected to contribute into the reaction. The barrier for the former, 16.2 kcal/mol, is slightly lower than the highest barrier at s-TS1, 19.0 kcal/mol, on the pathway leading to methanol. To estimate a possible branching ratio for formation of methanol and methyl radical in the reaction of palladium oxide with methane, we carried out transition state theory calculations with Wigner's tunneling correction[55] for the H-abstraction channel and for the rate-determining step of the methanol formation, PdO insertion into a C−H bond occurring at s-TS1 assuming efficient singlet−triplet intersystem crossing. For simplicity in both cases, PdO($^3\Sigma^-$) + CH$_4$ were taken as reactants, while t-TSa and s-TS1 served as transition states. The rate constants calculated for the 300−1000 K temperature range are plotted in Figure 7 and can be fitted by the following expressions (in cm^3 s^{-1} molecule^{-1}):

$$k_{\text{methanol}} = 5.60 \times 10^{-12} \exp(-20\,797/RT)$$

$$k_{\text{methyl}} = 7.12 \times 10^{-11} \exp(-17\,329/RT)$$

As one can see, the rate of the methyl radical formation is 2−3 orders of magnitude higher than the rate of the reaction channel proceeding via s-TS1 and eventually leading to the formation of CH$_3$OH. The branching ratio for the methanol channel is only 0.05% at 300 K and increases to 1.7% at 1000 K. Therefore, despite the fact that the barriers at t-TSa and s-TS1 differ by only ∼3 kcal/mol, the H-abstraction mechanism leading to PdOH + CH$_3$ dominates the reaction in the gas phase because it involves a looser transition state with lower vibrational frequencies (see Table S3 of Supporting Information).

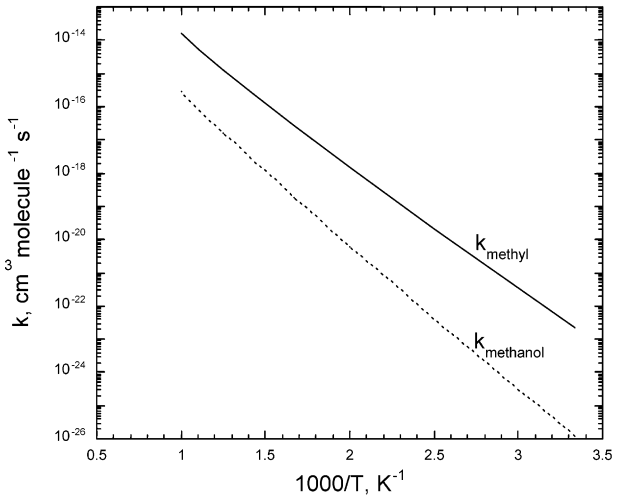

Figure 7. Arrhenius plots of calculated rate constants for H abstraction from CH$_4$ by PdO (k_{methyl}) and for insertion of PdO into methane's C−H bond (k_{methanol}).

On the other hand, methanol can be produced in a secondary reaction of PdOH with CH$_3$ via two channels, PdOH + CH$_3$ → s-CH$_3$PdOH → s-TS2 → s-PdCH$_3$OH → Pd(^{1}S) + CH$_3$OH (with the transition state lying 3.0 kcal/mol below reactants) and PdOH + CH$_3$ → s-PdCH$_3$OH → Pd(^{1}S) + CH$_3$OH.

The preference of the H-abstraction channel at higher temperatures is expected to be even more pronounced because this pathway does not involve nonadiabatic processes, e.g., singlet−triplet intersystem crossing. The spin−inversion process is more efficient at lower temperatures or/and lower kinetic energy excitations.[56] At higher temperatures, the spin−inversion probability is low due to the nonadiabaticity of the process and the insertion mechanism is expected to proceed by the PdO($^3\Sigma^-$) + CH$_4$ → t-CH$_4$PdO(l) → t-TS1 → t-CH$_3$PdOH → PdOH + CH$_3$ pathway. In this case, the reaction barrier is higher, 21.2 kcal/mol, and because the reaction continues within the triplet multiplicity, the only products are PdOH + CH$_3$ (see Figure 5). The situation for the PdO($^3\Sigma^-$) + CH$_4$ reaction is quite different from that for the FeO$^+$ + H$_2$ reaction, which was investigated by Filatov and Shaik.[56] In their case, the pathway of FeO$^+$ insertion into the H−H bond, designated as an addition−elimination mechanism, proceeds with spin−inversion via a sextet−quartet intersystem crossing point lying slightly lower in energy than the initial reactants. The abstraction pathway also goes through an intersystem crossing point, which resides ∼4 kcal/mol above the reactants. Hence, at low temperatures when the spin−inversion is efficient, the addition−elimination mechanism dominates the reaction. Alternatively, at higher temperatures, both addition−elimination and abstraction processes take the sextet multiplicity routes with similar activation barriers but the latter is more preferable because, according to TST calculations of the rate constants, it depicts a higher preexponential factor than the former. At intermediate temperatures, when the spin−inversion is still probable, the competition between the addition−elimination and abstraction pathways is more complex and both energetics (due to the height of the intersystem crossing points) and nonadiabatic effects are responsible for the branching ratio.[56]

Comparison of Methane Reactions with Various Metal Oxides and Metal Oxide Cations. Now we can compare the reaction mechanisms of CH$_4$ with oxides of an alkaline earth metal (BeO), an early transition metal (ScO), and two late transition metals (NiO, PdO). Among those, the scandium oxide appears to be the least reactive. At elevated temperatures, the

ScO + CH_4 reaction can produce the CH_3ScOH molecule and the molecular complex between scandium oxide and methane does not exist. ScO is not expected to assist the conversion of CH_4 into methyl radical or methanol. BeO is more reactive toward methane than NiO and PdO. The former can form a more stable molecular complex CH_4BeO bound by 20.7 kcal/mol[23] as compared to 9−10 kcal/mol for the complex formation energy of CH_4NiO and CH_4PdO. The barrier for the insertion into the C−H bond is 14.2 kcal/mol for BeO vs 28−29 kcal/mol for NiO and PdO. For the former, the insertion transition state lies lower in energy than BeO + CH_4 but the barriers relative to the initial reactants are 19−20 kcal/mol for NiO and PdO. For the reactions of BeO and NiO, the most favorable pathway for decomposition of the CH_3MOH intermediate is the cleavage of the M−C bond leading to the radical CH_3 + MOH products. For M = Be, this product channel is slightly exothermic (0.5 kcal/mol[23]) but for Ni, it is 13.2 kcal/mol endothermic. On the other hand, the CH_3PdOH molecule would decompose to Pd + methanol rather than to PdOH + CH_3 or PdO + CH_4.

The CH_3 + MOH products can be also formed by the direct abstraction of a hydrogen atom overcoming barriers of ∼16 kcal/mol for NiO and PdO, and this channel is expected to dominate the reactions. For BeO, this pathway is barrierless, but the reaction would most likely proceed by much more exothermic BeO + CH_4 → CH_4BeO → CH_3BeOH channel. If the CH_3BeOH molecule can be stabilized by collisions, it is expected to be the major reaction product, while a certain amount of BeOH and CH_3 can be also formed. Alternatively, the oxides of Ni and Pd can convert CH_4 to CH_3 at elevated temperatures. PdO is a better candidate for the methane conversion because, in addition to the production of CH_3, the recombination of PdOH with CH_3 should be facile and lead to the formation of methanol.

Some comparisons can be also made with the reactions of metal oxide cations, which were studied earlier both experimentally[10,11] and theoretically.[16−18] First, similar to the monoxide cations of the early transition metals, neutral ScO is not expected to activate methane. Second, for the late transition metals, the cations are able to form stronger complexes with CH_4, with the binding energies of 16.2, 22.8, and 26.5 kcal/mol for MnO^+, FeO^+, and CoO^+, respectively, as compared to 9−10 kcal/mol for NiO and PdO. Schröder and Schwartz[11] reported reaction efficiencies of transition metal oxide ions with methane as 100% for PtO^+, 40% for MnO^+, 20% for FeO^+ and NiO^+, and 0.5% for CoO^+. Yoshizawa et al.[18b] related these efficiencies to the barrier heights at TS1 with respect to the OM^+CH_4 reactant complex, which were computed as 9.4, 22.1, and 30.9 kcal/mol for MnO^+, FeO^+, and CoO^+, respectively. The corresponding values for NiO and PdO calculated here are 28−29 kcal/mol indicating that the reaction efficiency for the nickel and palladium oxide should be comparable or slightly better than that for CoO^+. However, this comparison may not be completely warranted since the dominant mechanism for the NiO + CH_4 and PdO + CH_4 reactions is the hydrogen abstraction pathway leading MOH + CH_3 with the barriers of ∼16 kcal/mol, i.e., lower than the barrier at TS1 for FeO^+. It is not clear so far what is the role of the H-abstraction mechanism in the MO^+ + CH_4 reactions, but apparently, it is not as important for the reactions of CoO^+, NiO^+, and PtO^+, which give mostly the M^+ + CH_3OH and MCH_2^+ + H_2O products formed via the HOM^+CH_3 intermediate. Also, in the FeO^+ + CH_4 reaction, Schröder and Schwartz[10] suggested $HOFe^+CH_3$ as a key intermediate based on the experimentally determined isotope effect. Additional theoretical calculations are needed in order to evaluate the branching ratios between the addition−elimination and abstraction mechanisms in the MO^+ + CH_4 systems. In terms of reaction selectivity, our results indicate that the reactions of NiO and PdO with methane would almost exclusively produce MOH and methyl radicals. In the reactions of cations, MnO^+ + CH_4 is also found to selectively form $MnOH^+$ + CH_3; CoO^+/NiO^+ + CH_4 give 100% of M^+ + methanol, while the reactions of FeO^+ and PtO^+ with methane produce a mixture of three products: MOH^+ + CH_3, MCH_2^+ + H_2O, and M^+ + CH_3OH.[11]

Conclusions

Density functional calculations of PES for the MO + CH_4 reactions (M = Sc, Ni, and Pd) show that the scandium oxide is not reactive with respect to methane at low and ambient temperatures. At elevated temperatures (when a barrier of ∼22 kcal/mol can be overcome), the reaction can produce the CH_3ScOH molecule but the latter is not likely to decompose to the methyl radical and ScOH or Sc + CH_3OH because of the high endothermicity of these processes. On the other hand, the oxides of nickel and palladium are more reactive and can form, without a barrier, molecular complexes with CH_4 stabilized by 9−10 kcal/mol. In addition, NiO and PdO can assist the methane conversion into free methyl radical and methanol at elevated temperatures. The dominant reaction channel is abstraction of a hydrogen atom from CH_4 with a barrier of ∼16 kcal/mol leading to MOH + CH_3. The recombination PdOH + CH_3 reaction is expected to further transform methyl radical into CH_3OH; however, the NiOH + CH_3 reaction is expected to produce only CH_3NiOH or to restore the initial reactants, NiO + CH_4. Summarizing, among the metal oxides considered here, PdO is the best candidate able to convert methane to free methyl radical and eventually to methanol through the gas phase reactions.

Acknowledgment. Funding from Tamkang University was used to buy the computer equipment used in part of this investigation. A partial support from Academia Sinica and the National Science Council of Taiwan, ROC, is also appreciated.

Supporting Information Available: Vibrational frequencies of various compounds in the ScO/NiO/PdO + CH_4 reactions calculated at the B3LYP/6-31G(d,p) level (Tables S1−S3) and details of the IRC calculations. This material is available free of charge via the Internet at http://pubs.acs.org.

References and Notes

(1) Lundsford, J. H. *Catal. Today* **2000**, *63*, 165.
(2) Shilov, A. E. *Metal Complexes in Biomimetic Chemical Reactions*; CRC: Boca Raton, 1996.
(3) Arndsten, B. A.; Bergman, R. G.; Mobley, T. A.; Peterson, T. H. *Acc. Chem. Res.* **1995**, *28*, 154.
(4) Crabtree, R. H. *Chem. Rev.* **1995**, *95*, 987.
(5) Lunsford, J. H. *Angew. Chem., Int. Ed. Engl.* **1995**, *34*, 970.
(6) Schneider, J. J. *Angew. Chem., Int. Ed. Engl.* **1996**, *35*, 1068.
(7) Hall, C.; Perutz, R. N. *Chem. Rev.* **1996**, *96*, 3125.
(8) Wang, H. Y.; Ruckenstein, E. *J. Catal.* **1999**, *186*, 181.
(9) Fox, J. M., III. *Catal. Rev. Sci. Eng.* **1993**, *35*, 169.
(10) Schröder, D.; Schwarz, H. *Angew. Chem., Int. Ed. Engl.* **1990**, *29*, 1433.
(11) Schröder, D.; Schwarz, H. *Angew. Chem., Int. Ed. Engl.* **1995**, *34*, 1973.
(12) Clemmer, D. E.; Chen, Y.-M.; Kahn, F. A.; Armentrout, P. B. *J. Phys. Chem.* **1994**, *98*, 6522.
(13) Siegbahn, P. E. M. *J. Am. Chem. Soc.* **1996**, *118*, 1487.
(14) Wittborn, A. M. C.; Costas, M.; Blomberg, M. R. A.; Siegbahn, P. E. M. *J. Chem. Phys.* **1997**, *107*, 4318.

(15) Musaev, D. G.; Morokuma, K. *J. Phys. Chem.* **1996**, *100*, 11600.
(16) (a) Fiedler, A.; Schröder, D.; Shaik, S.; Schwartz, H. *J. Am. Chem. Soc.* **1994**, *116*, 10734. (b) Danovich, D.; Shaik, S. *J. Am. Chem. Soc.* **1997**, *119*, 1773.
(17) Shaik, S.; Fiedler, A.; Schröder, D.; Schwartz, H. *Helv. Chim. Acta* **1995**, *78*, 1393.
(18) (a) Yoshizawa, K.; Shiota, Y.; Yamabe, T. *Chem. Eur. J.* **1997**, *3*, 1160. (b) Yoshizawa, K.; Shiota, Y.; Yamabe, T. *J. Am. Chem. Soc.* **1998**, *120*, 564. (c) Yoshizawa, K.; Shiota, Y.; Yamabe, T. *Organometallics* **1998**, *17*, 2825.
(19) (a) Kauffman, J. W.; Hauge, R. H.; Margrave, J. L. *J. Phys. Chem.* **1985**, *89*, 3541; 3547. (b) Park, M.; Hauge, R. H.; Margrave, J. L. *High Temp. Sci.* **1988**, *25*, 1. (c) Zhang, L. N.; Dong, J.; Zhou, M. F. *J. Phys. Chem. A* **2000**, *104*, 8882. (d) Zhou, M. F.; Zhang, L. N.; Dong, J.; Qin, Q. *J. Am. Chem. Soc.* **2000**, *122*, 10680; **2001**, *123*, 135. (e) Zhou, M. F.; Zhang, L. N.; Shao, L. M.; Wang, W. N.; Fan, K. N.; Qin, Q. *J. Phys. Chem. A* **2001**, *105*, 5801. (f) Zhang, L. N.; Zhou, M. F.; Shao, L. M.; Wang, W. N.; Fan, K. N.; Qin, Q. *J. Phys. Chem. A* **2001**, *105*, 6998.
(20) (a) Mascetti, J.; Tranquille, M. *J. Phys. Chem.* **1988**, *92*, 2177. (b) Burkholder, T. R.; Andrews, L.; Bartlett, R. J. *J. Phys. Chem.* **1993**, *97*, 3500. (c) Andrews, L.; Tague, T. J., Jr. *J. Am. Chem. Soc.* **1994**, *116*, 6856. (d) Chertihin, G. V.; Andrews, L. *J. Am. Chem. Soc.* **1995**, *117*, 1595. (e) Souter, P. F.; Andrews, L. *J. Am. Chem. Soc.* **1997**, *119*, 7350. (f) Zhou, M.; Andrews, L. *J. Am. Chem. Soc.* **1998**, *120*, 13230. (g) Galan, F.; Fouassier, M.; Tranquille, M.; Mascetti, J.; Papai, L. *J. Phys. Chem. A* **1997**, *101*, 2626.
(21) Greene, T. M.; Lansizera, D. V.; Andrews, L.; Downs, A. J. *J. Am. Chem. Soc.* **1998**, *120*, 6097.
(22) (a) Broclawik, E.; Yamauchi, R.; Endou, A.; Kubo, M.; Miyamoto, A. *J. Chem. Phys.* **1996**, *104*, 4098. (b) Broclawik, E.; Yamauchi, R.; Endou, A.; Kubo, M.; Miyamoto, A. *Int. J. Quantum Chem.* **1997**, *61*, 673.
(23) Hwang, D.-Y.; Mebel, A. M. *Chem. Phys. Lett.* **2001**, *348*, 303.
(24) Bärsch, S.; Schröder, D.; Schwarz, H.; Armentrout, P. B. *J. Phys. Chem. A* **2001**, *105*, 2005.
(25) Moore, S. E. *Atomic Energy Levels*; NSRDS: Washington, DC, 1971.
(26) *NIST Chemistry Webbook*; NIST Standard Reference DataBase Number 69, February 2000 release (http://webbook.nist.gov/chemistry/).
(27) Becke, A. D. *J. Chem. Phys.* **1993**, *98*, 5648.
(28) Lee, C.; Yang, W.; Parr, R. G. *Phys. Rev. B* **1988**, *37*, 785.
(29) Gonzalez, C.; Schlegel, H. B. *J. Phys. Chem.* **1990**, *94*, 5523.
(30) Hay, P. J.; Wadt, W. R. *J. Chem. Phys.* **1985**, *82*, 299.
(31) Dunning, T. H., Jr. *J. Chem. Phys.* **1971**, *55*, 716; **1970**, *53*, 2823.
(32) Ehlers, A. W.; Böhme, M.; Dapprich, S.; Gobbi, A.; Hölwarth, A.; Jonas, V.; Köhler, K. F.; Stegmann, R.; Veldkamp, A.; Frenking, G. *Chem. Phys. Lett.* **1993**, *208*, 111.
(33) Andrae, D.; Haussermann, U.; Dolg, U. M.; Stoll, H.; Preuss, H. *Theor. Chim. Acta* **1990**, *77*, 123.
(34) Dunning, T. H., Jr. *J. Chem. Phys.* **1989**, *90*, 1007.
(35) Cui, Q.; Musaev, D. G.; Morokuma, K. *J. Chem. Phys.* **1998**, *108*, 8418.
(36) Purvis, G. D.; Bartlett, R. J. *J. Chem. Phys.* **1982**, *76*, 1910.
(37) (a) Werner, H.-J.; Knowles, P. J. *J. Chem. Phys.* **1985**, *82*, 5033. (b) Knowles, P. J.; Werner, H.-J. *Chem. Phys. Lett.* **1985**, *115*, 259.
(38) (a) Werner, H.-J.; Knowles, P. J. *J. Chem. Phys.* **1988**, *89*, 5803. (b) Knowles, P. J.; Werner, H.-J. *Chem. Phys. Lett.* **1988**, *145*, 514.
(39) Frisch, M. J.; Trucks, G. W.; Schlegel, H. B.; Scuseria, G. E.; Robb, M. A.; Cheeseman, J. R.; Zakrzewski, V. G.; Montgomery, J. A., Jr.; Stratmann, R. E.; Burant, J. C.; Dapprich, S.; Millam, J. M.; Daniels, A. D.; Kudin, K. N.; Strain, M. C.; Farkas, O.; Tomasi, J.; Barone, V.; Cossi, M.; Cammi, R.; Mennucci, B.; Pomelli, C.; Adamo, C.; Clifford, S.; Ochterski, J.; Petersson, G. A.; Ayala, P. Y.; Cui, Q.; Morokuma, K.; Malick, D. K.; Rabuck, A. D.; Raghavachari, K.; Foresman, J. B.; Cioslowski, J.; Ortiz, J. V.; Baboul, A. G.; Stefanov, B. B.; Liu, G.; Liashenko, A.; Piskorz, P.; Komaromi, I.; Gomperts, R.; Martin, R. L.; Fox, D. J.; Keith, T.; Al-Laham, M. A.; Peng, C. Y.; Nanayakkara, A.; Gonzalez, C.; Challacombe, M.; Gill, P. M. W.; Johnson, B.; Chen, W.; Wong, M. W.; Andres, J. L.; Head-Gordon, M.; Replogle, E. S.; Pople, J. A. *Gaussian 98*, Revision A.7; Gaussian, Inc.: Pittsburgh, PA, 1998.
(40) MOLPRO is a package of ab initio programs written by H.-J. Werner and P. J. Knowles, with contributions from J. Almlöf, R. D. Amos, M. J. O. Deegan, S. T. Elbert, C. Hampel, W. Meyer, K. Peterson, R. Pitzer, A. J. Stone, P. R. Taylor, and R. Lindh.
(41) Wu, H.; Wang, L.-S. *J. Chem. Phys.* **1997**, *107*, 16.
(42) (a) Green, D. W.; Reedy, G. T.; Kay, J. G. *J. Mol. Spectrosc.* **1979**, *78*, 257. (b) Srdanov, V. I.; Harris, D. O. *J. Chem. Phys.* **1988**, *89*, 2748. (c) Ram, R. S.; Bernath, P. F. *J. Mol. Spectrosc.* **1992**, *155*, 315. (d) Namiki, K.; Saito, S. *Chem. Phys. Lett.* **1996**, *252*, 343. (c) Bakalbassis, E. G.; Stiakaki, M. A. D.; Tsipis, A. C.; Tsipis, C. A. *Chem. Phys.* **1996**, *205*, 389.
(43) Watson, L. R.; Thiem, T. L.; Dressler, R. A.; Salter, R. H.; Murad, A. *J. Phys. Chem.* **1993**, *97*, 5577.
(44) Bauschlicher, C. W., Jr.; Maitze, P. *Theor. Chim. Acta* **1995**, *90*, 189.
(45) Hwang, D.-Y.; Mebel, A. M. *Chem. Phys. Lett.* **2001**, *341*, 393.
(46) Hwang, D.-Y.; Mebel, A. M. *J. Phys. Chem. A* **2002**, *106*, 520.
(47) Hwang, D.-Y.; Mebel, A. M. *Chem. Phys. Lett.* **2002**, *357*, 51.
(48) Hwang, D.-Y.; Mebel, A. M. *J. Chem. Phys.* **2002**, *116*, 5633.
(49) Bauschlicher, C. W.; Nelin, C. J.; Bagus, P. S. *J. Chem. Phys.* **1985**, *82*, 3265.
(50) Schwerdtfeger, P.; McFeaters, J. M.; Moore, J. J.; McPherson, D. M.; Cooney, R. P.; Bowmaker, G. A.; Dolg, M.; Andreae, D. *Langmuir* **1991**, *7*, 116.
(51) Chung, S.-C.; Krüger, S.; Pacchioni, G.; Rösch, N. *J. Chem. Phys.* **1995**, *102*, 3695.
(52) Huber, K. P.; Herzberg, G. *Molecular Spectra and Molecular Structure. Constants of Diatomic Molecules*; Van Nostrand: New York, 1979.
(53) Merer, A. J. *Annu. Rev. Phys. Chem.* **1989**, *40*, 407.
(54) Schröder, D.; Shaik, S.; Schwarz, H. *Acc. Chem. Res.* **2000**, *33*, 139.
(55) Steinfeld, J. I.; Francisco, J. S.; Hase, W. L. *Chemical Kinetics and Dynamics*; Prentice Hall: Englewood Cliffs, NJ, 1999.
(56) Filatov, M.; Shaik, S. *J. Phys. Chem.* **1998**, *102*, 3835.